Biosensors and Bioelectronics 167 (2020) 112514

Contents lists available at ScienceDirect

Biosensors and Bioelectronics

journal homepage: http://www.elsevier.com/locate/bios

High-performance portable graphene field-effect transistor device for detecting Gram-positive and -negative bacteria

Kyung Ho Kim [a,1], Seon Joo Park [a,1], Chul Soon Park [a], Sung Eun Seo [a], Jiyeon Lee [a], Jinyeong Kim [a], Seung Hwan Lee [b], Soohyun Lee [a], Jun-Seob Kim [a], Choong-Min Ryu [a], Dongeun Yong [c], Hyeonseok Yoon [d], Hyun Seok Song [e], Sang Hun Lee [f,2,**], Oh Seok Kwon [a,g,*]

[a] Infectious Disease Research Center, Korea Research Institute of Bioscience and Biotechnology (KRIBB), Daejeon, 34141, Republic of Korea
[b] Department of Bionano Engineering, Hanyang University, Ansan, Republic of Korea
[c] Department of Laboratory Medicine and Research Institute of Bacterial Resistance, Yonsei University College of Medicine, Seoul, Republic of Korea
[d] School of Polymer Science and Engineering, Chonnam National University, 77 Yongbong-ro, Gwangju 61186, Republic of Korea
[e] Sensor System Research Center, Korea Institute of Science and Technology, Seoul, 02792, Republic of Korea
[f] Department of Bioengineering, University of California Berkeley, CA, 94720, USA
[g] Department of Nanobiotechnology, Korea University of Science and Technology (UST), Republic of Korea

ARTICLE INFO

Keywords:
Portable biosensor
Graphene field-effect transistor
Interfacing chemistry
Microfluidics
Real-time monitoring
Bioprobes

ABSTRACT

Current techniques for Gram-typing and for diagnosing a pathogen at the early infection stage rely on Gram stains, cultures, Enzyme linked immunosorbent assay (ELISA), polymerase chain reaction (PCR), and gene microarrays, which are labor-intensive and time-consuming approaches. In addition, a delayed or imprecise diagnosis of clinical pathogenic bacteria leads to a life-threatening emergency or overuse of antibiotics and a high-rate occurrence of antimicrobial-resistance microbes. Herein, we report high-performance antibiotics (as bioprobes) conjugated graphene micropattern field-effect transistors (ABX-GMFETs) to facilitate on-site Gram-typing and help in the detection of the presence or absence of Gram-negative and -positive bacteria in the samples. The ABX-GMFET platform, which consists of recognition probes and GM transistors conjugated with novel interfacing chemical compounds, was integrated into the microfluidics to minimize the required human intervention and facilitate automation. The mechanism of binding of ABX-GMFET was based on a charge or chemical moiety interaction between the bioprobes and target bacteria. Subsequently, ABX-GMFETs exhibited unprecedented high sensitivity with a limit of detection (LOD) of 10^0 CFU/mL (1–9 CFU/mL), real-time target specificity.

1. Introduction

Antibiotic medications are very important for treating or preventing bacterial infections by killing or inhibiting the growth of bacteria. Antimicrobial drugs have been used to treat a series of pathogenic infections and are applied to a wide variety of host organisms in animals and humans. However, the misuse and overuse of antibiotics in humans and animals can lead to a serious problem concerning the spread of antibiotic-resistant bacteria which cause untreatable infections (Currie et al., 2014; Kennedy et al., 2008; Kiraly et al., 2016; Li et al., 2016). The major reason for the overuse of antibiotics is the insufficient clinical information differentiating between Gram-positive bacteria (GPB) and Gram-negative bacteria (GNB) due to the absence of on-site rapid Gram typing or classifying technologies (Smith et al., 2018).

A technique, Gram statin, exists for Gram typing (Hu et al., 2018). Although this method is simple, easy to perform and highly accurate, the procedure is labor-intensive and time-consuming. Therefore, many biosensors for bacterial detection have been developed, such as colorimetric, cyclic voltammetry (CV), and fluorescence-based fluidic sensors. In particular, field-effect transistor (FET) methods have shown

* Corresponding author. Infectious Disease Research Center, Korea Research Institute of Bioscience and Biotechnology (KRIBB), Daejeon, 34141, Republic of Korea.
** Corresponding author. Department of Bioengineering, University of California Berkeley, CA, 94720, USA.
E-mail addresses: shlee.ucb@gmail.com (S.H. Lee), oskwon7799@gmail.com, oskwon79@kribb.re.kr (O.S. Kwon).
[1] These authors contributed equally to this work.
[2] Present Address: Department of Chemical and Biological Engineering, Hanbat National University, Daejeon 34158, Korea

https://doi.org/10.1016/j.bios.2020.112514
Received 9 May 2020; Received in revised form 9 August 2020; Accepted 11 August 2020
Available online 15 August 2020

impressive results, namely, rapid and accurate bacterial detection (Moudgil et al., 2020; Wu et al., 2017). However, these detection methods also have critical limitations, including i) necessitating a time-consuming process for discrimination, ii) having low accuracy with aged bacteria samples and iii) requiring specific fluorescent readers (Moscicki et al., 1987; Ouyang et al., 2015; Romero et al., 1988). Therefore, the development of alternative methodologies, that are capable of rapid, real-time, sensitive, selective, and multiplexed detection remains a challenge.

To date, various bioprobes used in analytical methods, including enzyme-linked immunosorbent assay (ELISA), lateral flow assays (LFAs), CV and chemiresistive or impedimetric sensors (García-Aljaro et al., 2010; Singh et al., 2019; Ugolini et al., 2018; Vaisocherová-Lísalová et al., 2016; Wang et al., 2018), have been introduced owing to their high sensitivity and specificity in bacterial detection. However, these bioprobes are suitable for detecting only previously identified bacteria, making them unsuitable for real-time monitoring. Recently, several antibiotics, such as natural antimicrobial peptides (AMPs), β-lactams, polymyxins and glycopeptides, were presented as bioprobes because of their high sensitivity and selectivity in the detection of Gram positive/negative bacteria in a mixture of bacterial strain. In particular, AMPs and glycopeptides have been highlighted owing to their unique property with strong affinity to the surface of bacteria. Therefore, various types of AMPs and glycopeptides have been studied for developing high-performance sensors.

In this study, we first demonstrated a real-time, portable device, namely, a dual antibiotics (as bioprobes)-conjugated graphene micropattern field-effect transistor (ABX-GMFET) combined with a microfluidic chip for discriminating bacteria at an early stage. Specifically, the bioprobes for identifying clinical GNB and GPB were founded by vancomycin and magainin I owing to their high affinity toward GPB and GNB groups. In addition, the novel chemical linkers, bis(2-aminoethylene)perylene-3,4,9,10-tetracarboxyldiimide (PDA) and 1-pyrenebutyric acid N-hydroxysuccinimide ester (PANHS), were synthesized to improve the immobilization capability of bioreceptors on GMs, as verified by density functional theory (DFT) calculations and 3D structure modeling. The real-time responses of liquid-ion gated ABX-GMFETs toward various bacteria showed high sensitivity and selectivity, and their maximal responses were clearly observed depending on the affinity for the bacteria (the limit of detection (LOD) of both ABX-GMFETs is approximately 10°–10^{1} CFU/mL). Moreover, the magainin I-conjugated GMFET (magainin I-GMFET) for GNB detection showed higher sensitivity than the vancomycin-conjugated GMFET (vancomycin-GMFET) for GPB detection with the same amount of bacteria. The Langmuir constants (K) were estimated by fitting the real-time responses and were used to evaluate the affinities for each species of bacteria. The high K values, 4.874×10^{-3} for GNB and 4.104×10^{-3} for GPB, indicate a strong intracellular affinity to the bioprobes. In addition, for the first time, an ABX-GMFET integrated into a dual-channel fluidic device showed high-resolution selectivity and sensitivity in the detection of bacteria from cultured samples, opening up the possibility of a portable ABX-GMFET system for on-site rapid bacterial Gram typing.

2. Materials and methods

2.1. Materials and apparatus

4-(4,6-Dimethoxy-1,3,5-triazin-2-yl)-4-methylmorpholinium chloride (DMTMM), vancomycin hydrochloride, 1,5-diaminonaphthalene (DAN) and PANHS were purchased from Sigma Aldrich Co., Ltd. Antimicrobial peptide maganinin I was synthesized by Lusen Sci, and polydimethylsiloxane (PDMS) was purchased from Dow Corning. Poly (methylmethacrylate), 950 PMMA A4 4% in anisole, was purchased from MicroChem Co., Ltd., and bacteria such as clinical isolates *Enterococcus faecium* EFM 13-7-9104, *Staphylococcus aureus* MSSA #94, *Escherichia coli* U238, *Klebsiella pneumoniae, Acinetobacter baumannii, Clostridioides difficile* and *Salmonella enterica* (serogroup) were obtained from clinical samples (IRB approval number 4-2017-1179). Atomic force microscopy (AFM) images were obtained with a Park NX10 system. High-resolution transmission electron microscopy (HR-TEM) images were obtained with an FEI Tecnai instrument, which can figure out the graphene layers. To measure HR-TEM, the graphene was performed by wet transfer process onto the copper grid. Raman spectra were measured with a BX41RF-LED instrument (Olympus, 633 nm laser).

2.2. PDA synthesis

Ethylene diamine (51.0 mmol) was added to a suspension of 3,4,9,10-perylenetetracarboxylic dianhydride (5.10 mmol) in toluene (100 mL). The reaction mixture was stirred and refluxed for 15 h and then filtered and washed with toluene. The crude dark red solid was added to 5 M KOH (100 mL) and stirred at room temperature (22 °C) for 6 h, and then the suspended reaction mixture was filtered and washed with water. The resulting red solid was dissolved in formic acid (100 mL) and filtered. Solidification was achieved in isopropanol (400 mL), and the product appeared as a dark brown solid (1.90 g, 78% yield). ^{1}H NMR (400 MHz, D_2O): δ 7.64–7.34 (br s, 8H), 4.22 (br s, 4H), 3.26 (br s, 4H). ^{13}C NMR (100 MHz, CF_3COOD): δ 167.89, 166.27, 136.09, 135.48, 133.08, 132.71, 129.38, 129.04, 126.23, 124.57, 124.33, 121.84, 40.90, 38.74 ppm. HR-MS (ESI+) calculated mass $C_{28}H_{21}N_4O_4$ [M + H^+] m/z 477.1557, found m/z 477.1561 (Fig. S1 and S2).

2.3. Graphene fabrication

Monolayer graphene (MLG) on a 4-inch wafer scale was grown on copper foil by using methane and hydrogen gas and was then transferred to the wafer through a graphene transfer process (Fig. S3 and S4).

2.4. DFT calculations

The GM sheet geometry was optimized with 96-carbon atoms. The Gaussian 09 W program was used for DFT calculations, and the calculations were performed using the B3LYP/6-31G(d) functional. To calculate the intermolecular distance, the molecular structures used 96-carbon GM sheets and single molecules of DAN and PDA, and the distance was calculated by Avogadro software.

2.5. Fabrication of the GMFETs

Graphene on a silicon dioxide (SiO_2) wafer was coated with an AZ 5214 E photoresist, and the photolithography process was performed through a film mask to create the graphene microchannel pattern (L = 20 μm, W = 50 μm). To design the GMs, the reactive-ion etching (RIE) process was introduced under the following conditions: O_2 50 sccm, 50 s, 50 mTorr, and 100 W power. The GM channel was recoated with DNR L-300-40 photoresist, and it was developed for source/drain electrode patterns. Cr/Au (1:10 ratio in thickness) was sequentially deposited by an electron beam (e-beam) evaporator. The electrode pathway was passivated with a SiO_2 layer with a 10 nm thickness to prevent nonspecific binding of analytes but the source/drain pads were opened as contact points with the probe tip (Fig. S5).

2.6. Bioprobe immobilization on the GMs

For detection of GNB, 10 μL of 10 μM PDA (in distilled water (DW)) was used to treat the GM channel for 1 h. After, that the channel was washed with pH 7.4 PBS solution and DW. The amine-functionalized GM was treated with 5 μL of 1 wt% DMTMM (in DW) and 5 μL of 10 μg/mL magainin I (in DW) over 4 h at 4 °C and then washed with PBS solution and DW. For detection of GPB, 10 μL of 10 μM PANHS (in DW) was added to the GM channel and allowed to sit for 1 h. Then, the cells were washed with PBS solution and DW. PANHS-functionalized graphene was

treated with 5 μL of 10 μg/mL vancomycin (in DW) over 4 h at 4 °C and then washed with PBS solution and DW (Fig. S6).

2.7. Fluorescence measurements

The bioprobes were labeled with fluorescein-5-isothiocyanate (FITC) at each terminal functional group as follows: the amine group of magainin I and the carboxyl group of vancomycin. Green fluorescence-labeled bioprobes were immobilized in the electrode channels, and fluorescence images of the channels were obtained by an Evos FL instrument (Thermo Fisher Scientific Corporation).

2.8. Fabrication of the GMFET fluidic chip

The Si wafer was coated with the SU8-3035 photoresist for 15 min at 95 °C, and photolithography was performed *via* a film mask to produce the microfluidic channel pattern; the wafer was then baked for 1 min (at 60 °C) and 5 min (at 95 °C). The PDMS of the base and curing agent (10:1 ratio) was allowed to swell on the GM substrate, which was baked in a 90 °C oven over 2 h. The PDMS chip with microfluidic channels was treated with O_2 plasma under the following conditions: O_2 30 sccm, 60 s, 100 W generation power and 7E-1 mTorr. The clean PDMS chip was attached to the GMFET device (Fig. S7).

2.9. Electrical measurements of the ABX-GMFET

All electrical measurements were performed by a Keithley 2612 A source meter and a probe station (MS-tech, model 4000) under biosafety level 2 (BSL2) laboratory conditions. The current change was normalized based on the following equation: $\Delta I = (I/I_0)/I_0$, where I_0 is the initial current and I is the measured current in real time.

2.10. Bacterial sample preparations

Bacteria were identified by matrix-assisted laser desorption and ionization time-of-flight (MALDI-TOF) (Bruker Biotyper MS, Bruker Daltonics, Bremen, Germany) and 16 S rRNA gene sequencing and were kept at −70 °C until they were used. To identify bacteria species, conventional 16 S ribosomal RNA gene sequencing technique was employed and performed by Genotech. Inc. (Daegeon, S. Korea), then, analyzed by BLAST searches of the NCBI database. All bacterial strains were grown to the stationary phase in Luria-Bertani (LB) broth at 37 °C and 250 rpm for 16 h. Cell numbers were determined by counting the colony forming units (CFU). All kinds of bacteria were cultured in LB agar medium for 16 h, and the collected bacteria cells were resuspended in sterilized water to a final concentration with an optical density (OD) 600 = 1, as measured using a spectrophotometer. The media of cultured bacteria was exchanged with PBS solution, afterward, which was serially diluted using PBS solution until 10^0 CFU/mL. For confirm of colony counting, the diluted bacterium was cultured for 12 h after spreading on the LB agar medium.

2.11. Assembly of a portable GMFET device

The hardware printed circuit board (PCB) of the device was composed of a microcontroller (QFN-48), a digital-to-analog converter (DAC8832) and an analog-to-digital converter (7192 CE) and was located on the middle layer. For the source power supply, a portable battery was used on the bottom layer and was connected to a charge pump (LM27762), a reference (REF2925) and a low-dropout regulator (AAT3237). The top layer, for loading GMFET fluidics chip, consisted of a source, drain and gate, which were connected *via* wiring to the microcontroller.

3. Results and discussion

3.1. Development of the dual ABX-GMFET microfluidic chip

The illustration in Fig. 1 presents the overall bacterial discrimination system based on the dual ABX-GMFETs integrated with a microfluidic chip, which consists of a PDMS microfluidic channel, a graphene transistor and electrodes (Fig. 1A, right side). The following bacteria-specific bioprobes were introduced onto the GM surface by interfacial reagents: i) vancomycin for GPB and ii) magainin I for GNB (Fig. 1B). Moreover, both the bioprobes on the GMFETs showed ultrahigh affinity, resulting in excellent selectivity and sensitivity (Fig. 1C). Four types of bacterial species, *Escherichia coli* (*E. coli*), *Salmonella enterica* (*Salmonella*), *Staphylococcus aureus* (*S. aureus*) and *Enterococcus faecium* (*E. faecium*), were introduced as cultured samples of pathogens consisting of GPB and GNB groups. To identify each target bacteria with the ABX-GMFETs, a portable multiplexed platform with a dual ABX-GMFET channel was introduced and used to measure a bacterial mixture to compare the Langmuir constants (K) of each ABX-GMFET.

3.2. Characterization of MLG

Generally, MLG has various electrical properties, such as zero-bandgap semiconducting properties, high-field transport and high carrier mobility (Allen et al., 2010; Avouris and Dimitrakopoulos, 2012). Therefore, various applications with MLG have been developed, and MLG has shown excellent electrical performance (Kwon et al., 2015, 2013; Park et al., 2012). FET-based chemo-/biosensors, especially liquid-ion gated FET biosensors, are a type of MLG-containing electronic device (Bolotin et al., 2008; Frank, 2010; Kwon et al., 2019). To determine the number of graphene layers, the graphene sample was analyzed by HR-TEM. As shown in Fig. 2A, the HR-TEM image shows the MLG and hexagonal structure lattice of graphene at high magnification (right image of Fig. 2A). Moreover, selected area electron diffraction (SAED) patterns showed the hexagonal ring patterns expected of MLG (the inset of Fig. 2A) (Seo et al., 2017). Raman spectroscopy was also used to investigate the characteristics of the graphene layer based on the 2D/G peak intensity ratio, and the I_{2D}/I_G value of the graphene that underwent chemical vapor deposition (CVD) was determined to be approximately 1.98 (Fig. 2B). Fig. 2C displays the GM channel between the electrodes fabricated by a microelectromechanical system (MEMS) (Fig. S3), which was passivated with a photoresist to endow the Au surface with environmental stability from the surrounding liquid phase. Moreover, the purpose of electrode passivation was to minimize the noise current level caused by the physical absorption of nontarget analytes on the Au surface. AFM analysis showed an obviously different height of the GM on silicon dioxide, and the height was approximately 1.1 nm in area *A3* (the inset of Fig. 2C) (Pampaloni et al., 2018). Fig. 2D compares the Raman spectra of GM (*A2*) in the different areas on SiO_2 (*A1*) shown in Fig. 2C. The G and 2D peaks are clearly observed, with I_{2D}/I_G values of approximately 1.95, for only area *A2*. GM can be confirmed to be completely formed by the etching process on the SiO_2 substrate. Therefore, the transducer of FET-type biosensors can be constructed by GM channels between the source and drain electrodes.

3.3. Characterization of interfacial chemistry

One of the most critical factors in GMFET biosensors is the introduction of efficient interfacial chemical compounds that control the position of the active site placed in the bioprobes, because magainin I and vancomycin have different active sites, leading to high-performance GMFET biosensors. DAN has been commonly used as a linker for GFETs because of its easy functionalization. However, DAN has a critical limitation: its end groups (the amine moieties) are parallel to the graphene surface. Therefore, the bioreceptors are partially bound to the functional group of DAN due to steric hindrance, and the active sites of the

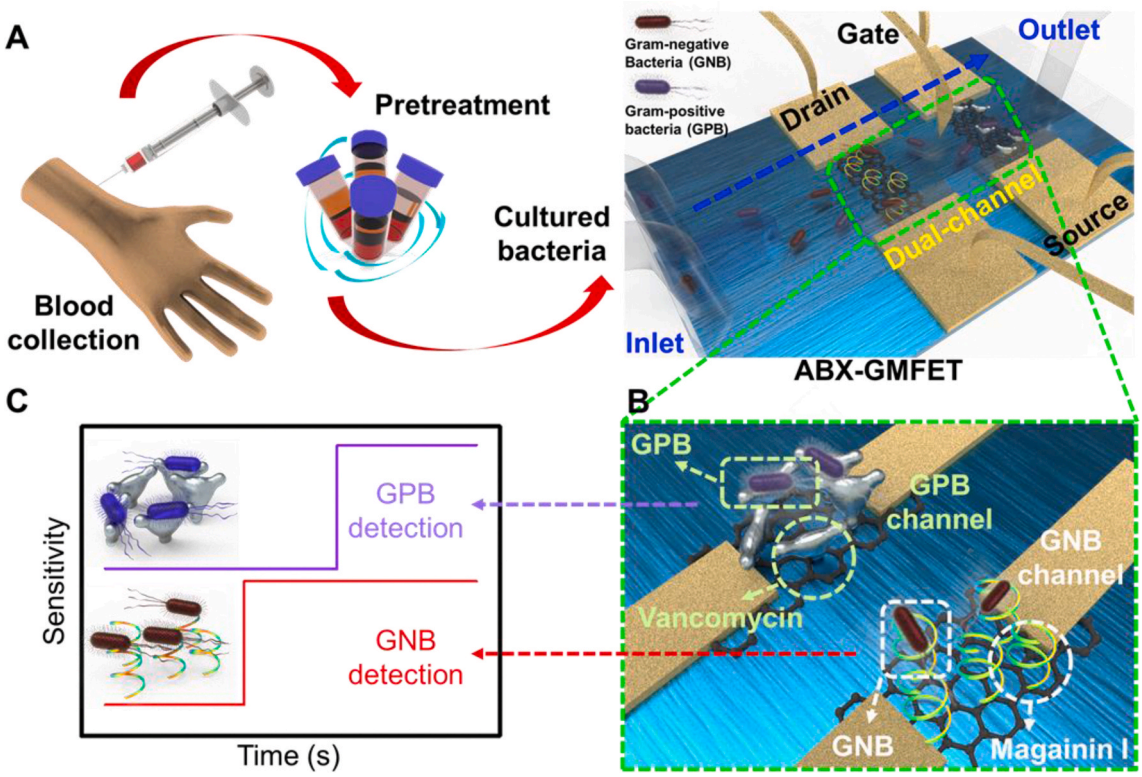

Fig. 1. Schematic illustrations of (A) whole system of ABX-GMFET with dual-channels for discriminating GPB and GNB in pretreated cultured samples and (B) the extended ABX-GMFET dual channels with bioprobes such as vancomycin and magainin I *via* interfacial chemicals and linkers. (C) Real-time responses with electrical signals by specific detection between bioprobes and GPB/GNB.

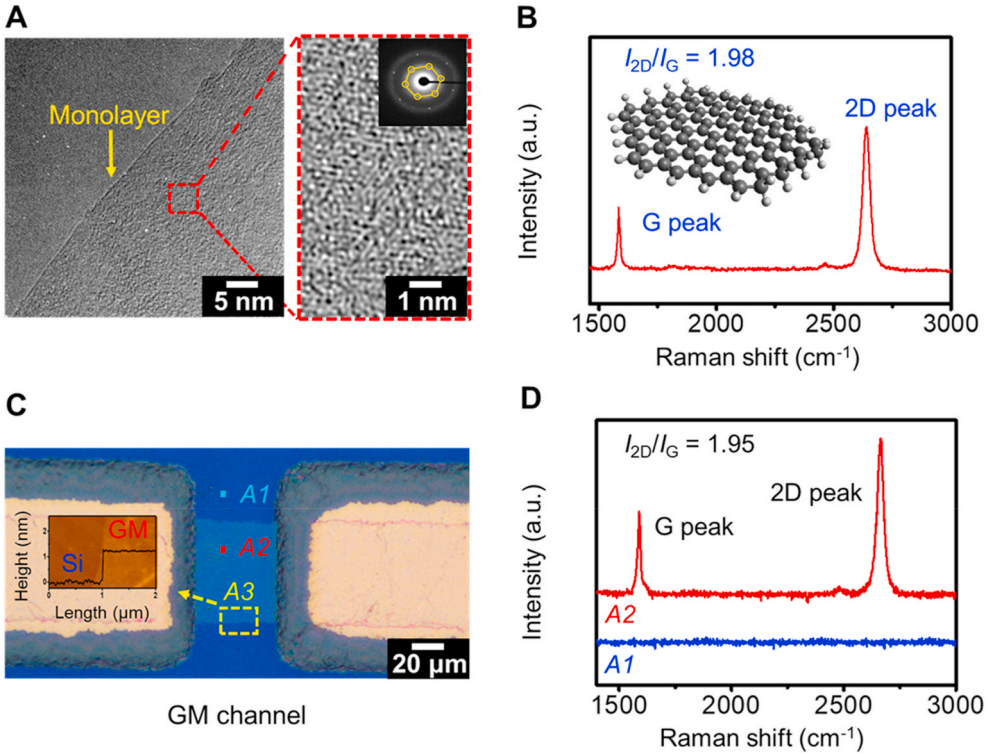

Fig. 2. MLG characterizations: (A) HR-TEM image of MLG and its hexagonal structure in the SAED image (insert). (B) Raman spectra of MLG (I2D/IG ratio = 1.98). (C) Optical image of the GM channel between passivated Au/Cr electrodes (the inset indicates the AFM image in the A3 area). (D) Raman spectra comparison in the A2 and A1 regions to identify the existence of the GM channel.

bioreceptors are randomly exposed to target bacteria leading to a reduction in the interaction between magainin I and GNB (An et al., 2013; Cuervo et al., 1988). To replace DAN, PDA was synthesized and characterized (Fig. S1 and S2). To compare the stacking structure of PDA and DAN on the GM, DFT calculations were performed using B3LYP (Fig. 3A) (Im et al., 2017). The intermolecular interaction between each linker and the GM was confirmed by DFT calculation using the B3LYP functional with a split-valence basis set (6-31G(d)) (Table S1). The absolute energies of each molecule are as follows: GM = - 98,117 eV, DAN = - 13248.2 eV, and PDA = - 42659.7 eV. The interaction energies were calculated with the following equation.

$$\Delta E = E_{GM/\text{linker}} - [E_{GM} + E_{\text{linker}}] \quad (1)$$

where $E_{GM/linker}$, E_{GM} and E_{linker} indicate the total energy of the π - π interactions, the energy of GM and the energy of DAN or PDA. The calculated intermolecular interaction energies were - 111,365 eV for DAN and - 140,777 eV for PDA. Based on these results, the π - π interaction energy of the GM with PDA (ΔE = - 0.14183 eV) was confirmed to be stronger than that of the GM with DAN (ΔE = - 0.04166 eV). Therefore, PDA was used as a linker for conjugating magainin I onto the GMFET platform. In addition, in Fig. 3A, the amine groups of PDA exhibit vertical orientation compared to those parallel to DAN. Therefore, PDA was introduced as a linker for magainin I to maximize the activity of bioprobes on the GMFETs. Magainin I has two terminal groups in its chemical structure: i) amine (N terminus) and ii) carboxylic (C terminus) groups. The C terminus of magainin I was used to construct amide bonds with the amine groups of PDA, while the N terminus was fully available to promote bioprobe activity (Fig. 3B). The active site of vancomycin is distributed *via* the positively charged zone (see the violet circle in Fig. 3C), and its activity is also maximized by forming an amide bond with the amine group indicated in Fig. 3C. Therefore, PANHS was utilized on the GM because the pyrene backbone enables stacking of the GM, as NHS easily forms amide bonds with the amine groups of vancomycin (Fig. S4) (Ping et al., 2016).

3.4. Characterization of immobilized bioprobes

To investigate the pristine GM and linker-treated GMs, X-ray photoelectron spectroscopy (XPS) analysis was conducted. The intensity of the C 1s peak obviously increased upon functionalization of the GM surface with interfacial chemical compounds, as shown in Fig. 4A. There was no significant N 1s peak in the spectrum of the pristine GM; however, the linker-GMs obtained after surface treatment with PDA and PANHS were observed to have nitrogen peaks at approximately 398 eV for PANHS-GM and at approximately 397 eV for PDA-GM (Fig. S8) (Liu et al., 2014). Fourier transform infrared (FT-IR) spectroscopy was carried out to examine the successful chemical bonding between the bioprobes and linkers on the GMs. The absorption peaks from 1700 cm^{-1} to 1200 cm^{-1} were attributed to the bending vibrations of the amine, alkyl and carbonyl groups, and the peaks in the range from 3300 cm^{-1} to 3200 cm^{-1} were confirmed to be broad bands corresponding to the –OH and –NH groups. At 1700 cm^{-1} and 1480 cm^{-1} and in the range from 1400 cm^{-1} to 1200 cm^{-1}, the FT-IR spectrum displayed sharp –C═O and strong -C-N bands. Generally, the absorption peaks of the amide I and II bands are located in the ranges from 1700 to 1600 cm^{-1} and from 1580 cm^{-1} to 1480 cm^{-1}, respectively. Interestingly, the intensities of the amide I and II bands were significantly increased for PDA-magainin I

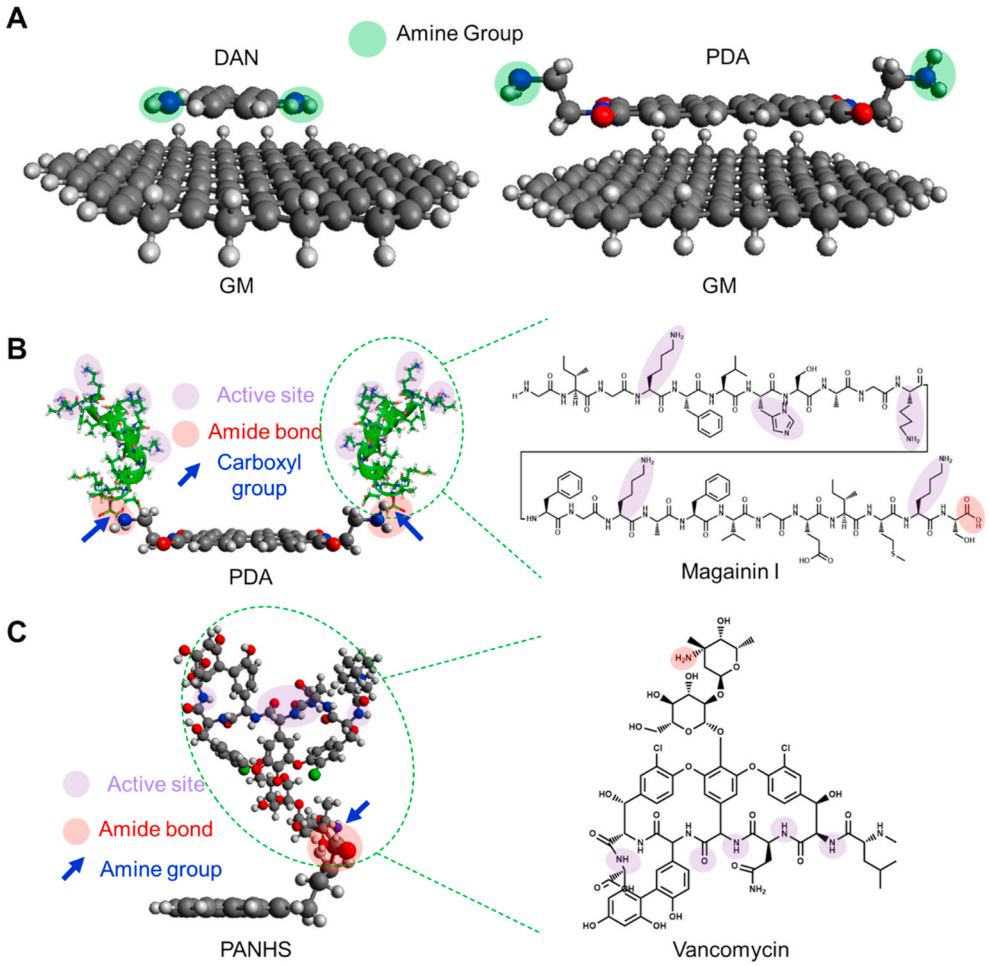

Fig. 3. (A) DFT-based intermolecular interaction structure of the GM with linkers (DAN (left) and PDA (right)). (B) Chemical structure of PDA combined with magainin I (the extended chemical structure). The violet circles in the magainin I structure indicate active sites. (C) Chemical structure of PANHS combined with vancomycin (the extended chemical structure). The violet circles also show the active sites in the vancomycin structure. (For interpretation of the references to color in this figure legend, the reader is referred to the Web version of this article.)

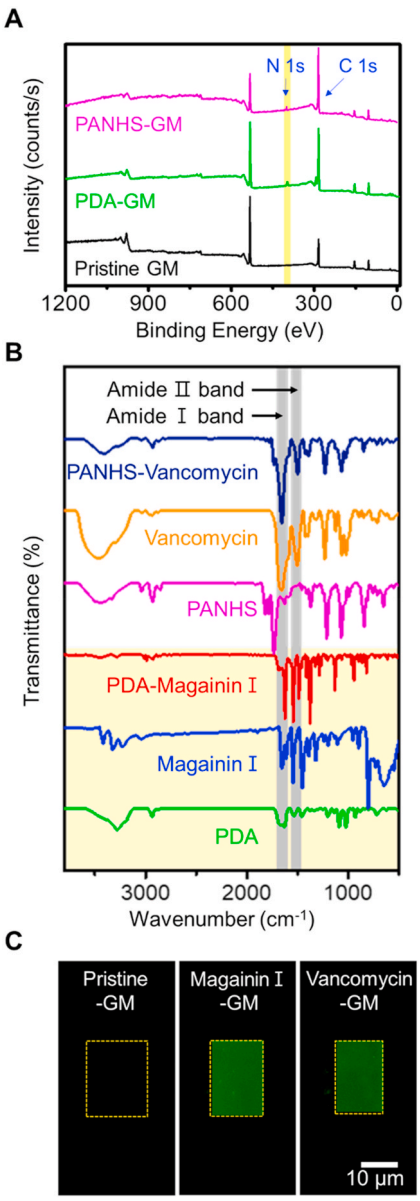

Fig. 4. Characterization of bioprobe immobilization on the GM surface. (A) XPS spectra of each linker functionalized on the GM surface. (B) FT-IR spectra of each bioprobe immobilization process with linkers and bioprobes on the GM surface. (C) Fluorescence images of pristine graphene (left) and the GM on which magainin I (middle) and vancomycin were immobilized (right).

compared to those of magainin I. These absorption peaks were also observed in the spectrum of PANHS-vancomycin. These results indicated that the specific linkers were successfully coupled with the bioprobes on the GM surface (Fig. 4B). Furthermore, FITC was used to label the bioprobes to obtain fluorescence images of the bioprobe linkers on the GM channels. The fluorescence images exhibited green fluorescence in both the pristine GM and bioprobe-treated GM channels between the source and drain electrodes (Fig. 4C).

3.5. Electrical property characterization of ABX-GMFETs

To examine the electrical properties of the ABX-GMFETs, one of the most efficient methodologies is liquid-ion gating (Song et al., 2013), which enables intimate contact *via* a remote gate electrode in the surrounding electrolyte solution of phosphate-buffered saline (PBS, pH 7.4). Moreover, this strategy has been introduced for signal amplification to enhance the sensing performance of resistive sensors. The schematic illustration in Fig. 5A shows the liquid-ion gated ABX-GMFET, which is composed of source, drain and gate electrodes for electrical measurements. In addition, the liquid in the chamber, as a dielectric, promotes the formation of a field effect by the supplied gate voltage. The current-voltage (*I–V*) curves of pristine GM, the GMs with linkers (PDA and PANHS) and the ABX-linker-GMs (magainin I-PDA-GM and vancomycin-PANHS-GM) displayed a linear correlation in the range from - 2.5 V to + 2.5 V (scan rate = 0.01Vms^{-1}), which indicates that the gradient changes depend on the immobilized probe molecules (Fig. 5B). The current level was slightly decreased by consecutive steps of bioprobe introduction *via* physical and chemical attachment onto the materials, showing clear ohmic behaviors according to Ohm's law (Fig. S9).

According to our previous works, the conductance of GM transistors exhibits ambipolar behavior and the p-type region is suitable for liquid-ion gated biosensors because of the electron-transfer by oxygen in the liquid state (Fujimoto and Awaga, 2013). Therefore, to establish the range of p-type operation of ABX-GMFETs, the output curves were characterized. The output curves of both ABX-GMFETs are displayed according to the gating effects: I_{ds} negatively increased with a negative increase in gate voltage (in the range of V_{ds} = 0 to −0.5 V) (Fig. 5C and D). These results indicate hole-transport behavior, resulting in p-type transistor characteristics. Moreover, the sensing mechanism of ABX-GMFETs toward GNB and GPB was characterized based on a transfer curve analysis (Fig. 5E and F). Positive charge carriers accumulate on the surface of the pristine GM by increasing the negative charge in the liquid-ion gated dielectric. The minimum gating effect ($V_{g,min}$) on the GM was calculated with the Dirac point in the transfer curve of histidine of the GM transistor, and the molecular gating effects were demonstrated by the shifts in $V_{g,min}$. The initial $V_{g,min,GM}$ of the pristine GM was approximately 0.88 V and the $V_{g,min,linkers}$ values after introduction of the linkers with PDA and PANHS displayed negative shifts, $V_{g,min,PDA}$ = 0.68 V and $V_{g,min,PDNHS}$ = 0.81 V, owing to the positive charges of the amine groups on PDA and the n-doping effect of PANHS (Ghosh et al., 2018). Moreover, the attachment of magainin I and vancomycin on the linkers-GMs enabled the shift to more negative values for $V_{g,min,ABXs}$. This observation is explained by the fact that magainin I consists of cationic groups, such as lysine and histidine, and vancomycin has a positive charge of approximately +0.67 at pH 7.4 (Takacsnovak et al., 1993); the isoelectric point (pI) of vancomycin is pH 8.3 (Johnson and Yalkowsky, 2006), resulting in negative shifts in $V_{g,min,ABXs}$. Therefore, the total fabrication processes of ABX-GMFETs led to a negative shift in the transfer curve. However, the real-time responses of ABX-GMFETs toward representative cultured samples, such as *E. coli* and *S. aureus*, at a concentration of 10^3 CFU/mL showed complementary positive shifts in the $V_{g,min}$ (0.57 and 0.75 V) values because the surface of the bacteria had negative charges (Gonçalves and de Carvalho, 2016; Li and McLandsborough, 1999). Based on the electrostatic gating effects of the ABX-GMFETs (Kwon et al., 2015), this platform can be utilized for monitoring real-time responses to bacterial mixtures with various concentrations.

3.6. Real-time monitoring of liquid-ion-gated ABX-GMFETs

To confirm the bacteria-sensing performance of the ABX-GMFETs, the liquid-ion-gated geometry was designed by MEMS technology. The two GM channels were combined with magainin I, which detects only GNB, and their real-time responses were measured (Fig. 6A–C), while vancomycin was introduced on the GMs for GPB detection (Fig. 6D–F). Upon sequential addition of bacteria, the current levels of the ABX-GMFET increased with increasing mixture concentration at different current change ratios. The current change was normalized by the equation

$$\Delta I / I_0 = (I - I_0)/I_0 \quad (2)$$

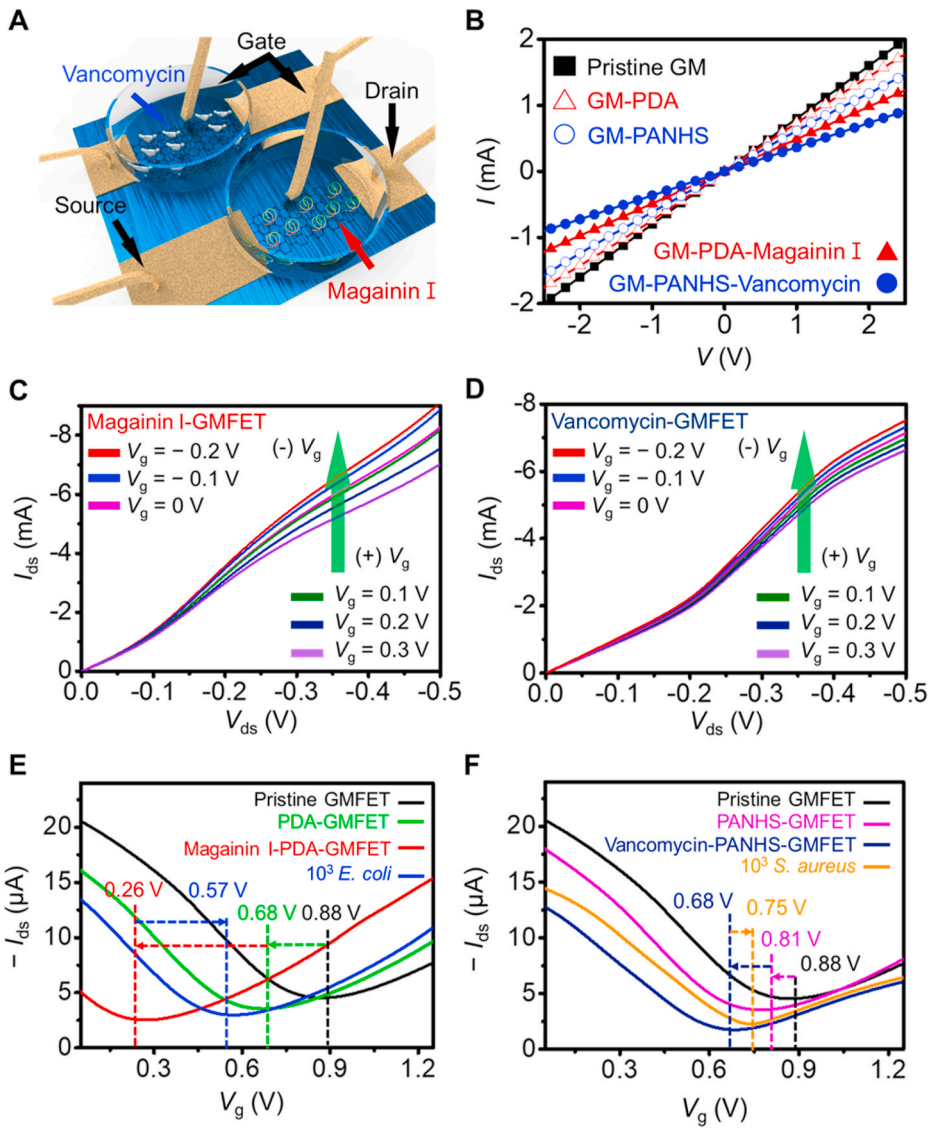

Fig. 5. Characterization of the electrical properties of ABX-GMFETs. (A) Schematic illustration of the liquid-ion-gated ABX-GMFETs in the reaction chamber, which consisted of a source/drain and gate electrodes. (B) Current-voltage (I–V) curves of each step in the bioprobe immobilization processes on the GM surface. The red and blue lines represent magainin I-PDA-GM and vancomycin-PANHS-GM channels, respectively (V_g = 0 V, scan rate = 0.01 Vms^{-1}). I_{ds}-V_{ds} output characteristics of ABX-GMFETs with (C) magainin I and (D) vancomycin in ranging from - 0.2 V to 0.3 V in a step 0.1 V of gate voltage (V_{ds} = 0 to – 0.5 V, scan rate = 0.01 Vms^{-1}). (E and F) The $V_{g,min}$ measurements of each modification process of magainin I-GMFET for the GNB channel and vancomycin-GMFET for the GPB channel (V_{ds} = - 1 mV). A shift in the $V_{g,min}$ values occurs by adding target bacteria (*E. coli* and *S. aureus*) for each ABX-GMFET. (For interpretation of the references to color in this figure legend, the reader is referred to the Web version of this article.)

where I_0 and I represent the current changes before and after exposure to the target bacteria, respectively. To confirm the interaction between the bioprobes and the target bacteria, control experiments were carried out with electrodes that were not surface modified with bioprobes (Fig. S11). Fig. 6A displays the real-time responses of the magainin I-GMFET to various concentrations ranging from 10^0 to 10^4 CFU/mL of the living cultured GNB: *E. coli* (red line) and *Salmonella* (blue line). Before monitoring the signal of bacteria, only buffer without any bacteria was injected and there was no signal. Otherwise, changes in current, which were explained by the electrostatic gating effects, were observed immediately after bacterial injection, with a response time within approximately 5 s, and the LOD of the magainin I-GMFET was approximately 10^0 CFU/mL. This LOD is 10 times more than that of conventional GNB biosensors (Table S2). Although *E. coli* and *Salmonella* are classified into the same group of GNB, different signal intensities in response to these two species were observed due to the different degrees of affinity of magainin I toward *E. coli* and *Salmonella* (Dickson and Koohmaraie, 1989). In particular, *E. coli* and *Salmonella* are specific targets of magainin I, which is a conventional AMP; AMPs have been characterized as broad spectrum bioprobes against many GNB and have strong binding affinities for the surface of bacteria (Chen et al., 2014; Shai, 1999). The real-time responses of the magainin I-GMFET to *E. coli* exhibited a higher current intensity level than those of the magainin I-GMFET to *Salmonella* because the outer membrane (lipopolysaccharide (LPS) layer) of *E. coli*. has a larger negative charge distribution than that of *Salmonella* (Soni et al., 2008). To confirm the cross-reactivity of magainin I with Gram-positive species, the GMFET conjugated with magainin I was exposed to GPB, namely, *S. aureus* and *E. faecium*. As shown in Fig. 6B, no significant responses to approximately 10^3 CFU/mL GPB were observed. In addition, the dose-response toward various concentrations of GNB was determined, and the normalized sensitivities were calculated by the current change level. The K values were calculated by Langmuir's adsorption isotherm equation based on the fitting curve

$$N = C/(1/K + C) \quad (3)$$

where C is the concentration of bacteria and N is the normalized sensitivity (Kwon et al., 2015; Lee et al., 2011; Oh et al., 2019; Park et al., 2017, 2012). The obtained K values were 4.874×10^{-3} for *E. coli* and 4.077×10^{-3} for *Salmonella*. Although the two types of GNB have equal negative charges, the K values are significantly different due to the quantity of negative charge on the outer bacterial membrane (Fig. 6C) (Wakshlak et al., 2015).

To screen the Gram-positive species, ABX-GMFET channels were prepared and conjugated with vancomycin, which strongly adsorbs GPB,

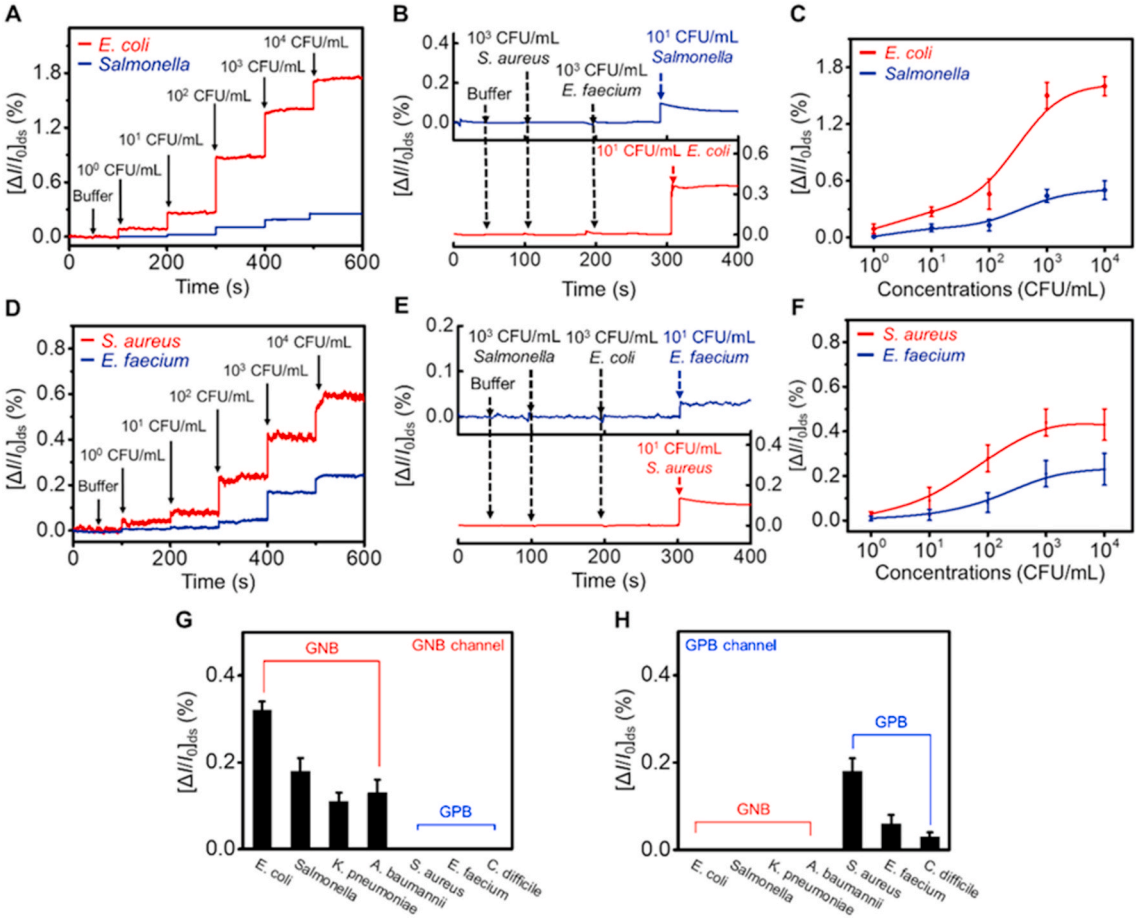

Fig. 6. (A) Real-time responses of the liquid-ion-gated magainin I-GMFET toward various GNB concentrations (10^0 CFU/mL to 10^4 CFU/mL), such as *E. coli* (red line) and *Salmonella* (blue line), where V_{ds} = - 1 mV and V_g = - 0.1 V. (B) Specificity of the magainin I-GMFET toward target GNB (*E. coli* and *Salmonella*) and nontarget GPB (*S. aureus* and *E. faecium*). (C) Calibration curves of the magainin I-GMFETs toward the GNB. (D) Real-time responses of the liquid-ion-gated vancomycin-GMFET toward various GPB concentrations (10^0 CFU/mL to 10^4 CFU/mL), such as *S. aureus* (red line) and *E. faecium* (blue line), where V_{ds} = - 1 mV and V_g = - 0.1 V. (E) Specificity of the vancomycin-GMFET toward target GPB (*S. aureus* and *E. faecium*) and nontarget GNB (*E. coli* and *Salmonella*). (F) Calibration curves of the vancomycin-GMFET toward GPB. (G, H) Response intensity of various bacterial species at a concentration of 10^0 CFU/mL in each channel (n = 3). There were no significant signals of GPB in the GNB channel or GNB in the GPB channel. (For interpretation of the references to color in this figure legend, the reader is referred to the Web version of this article.)

including *S. aureus* and *E. faecium*. The bacteria-specific interaction of vancomycin involves binding of the D-Ala-D-Ala terminus of the peptidoglycan to the outer membrane of GPB because these bacteria have a high affinity for D-Ala-D-Ala, thus forming a network of five hydrogen bonds with vancomycin (Walsh, 1993). Fig. 6D presents the real-time responses of the vancomycin-GMFET to living clinical GPB operated by electrostatic gating effects. The LOD of vancomycin-GMFET was similar to that of magainin I-GMFET, which was approximately 10^0 CFU/mL for *S. aureus* and *E. faecium*, and the current values were measured within approximately 5 s. These results also showed over 10 times better detection performance than conventional GPB biosensors (Table S2). Although there were significant signals from the vancomycin-GMFET in response to both *S. aureus* and *E. faecium*, the sensitivities were monitored with different intensities because the minimum inhibition concentration (MIC) value of *E. faecium* (0.5–64.0 μg/mL) is higher than that of *S. aureus* (0.25–1.0 μg/mL) (Rybak et al., 1998). Moreover, to characterize the excellent selectivity of ABX-GMFET platforms, the bacterial specificity of the vancomycin-GMFET was demonstrated with nontarget GNB and target GPB. Fig. 6E shows the specificity of the vancomycin-GMFET for GPB at approximately 10^1 CFU/mL, which were sequentially added in the following order: *Salmonella*, *E. coli* and both *S. aureus* and *E. faecium*. The vancomycin-GMFET displayed no significant responses to GNB, even at a high concentration of approximately 10^3 CFU/mL. However, clear responses were observed to the GPB approximately 10^1 CFU/mL. The vancomycin-GMFET had excellent sensitivity values of approximately 0.13% and 0.05% toward *S. aureus* and *E. faecium*, respectively. These results confirmed that even coexisting nontarget bacteria at low to high concentrations had no significant effects, which indicates the absolute specificity of the ABX-GMFET platform. In addition, the *K* values were calculated with the same equation used in Fig. 6F, and the *K* constants for *S. aureus* and *E. faecium* were determined to be 4.104×10^{-3} and 3.426×10^{-3}, respectively. The *K* constants were correlated with the MIC values of vancomycin for these bacteria (Fig. 6F). Based on all of the *K* values, the intensities of the ABX-GMFETs toward various bacteria could be ranked, as shown in Table S3. Among these bacteria, the highest *K* value was 4.874×10^{-3} for *E. coli*, while the lowest *K* value was 3.426×10^{-3} for *E. faecium*. Therefore, the magainin I-conjugated GMFET had the strongest adsorption interaction with *E. coli*, and this interaction was stronger than that of the vancomycin-GMFET toward GPB. Moreover, to confirm the reactivity regarding various bacterial species, specificity tests with GNB and GPB panels were performed to measure the electrical responses. The ABX-GMFET sensors specifically responded to each channel as shown in Fig. 6G and H and S10. The reproducibility and storage stability of ABX-GMFETs were evaluated by the long-term stability over 15 days, and their sensitivity decreased to

approximately 10% as shown in Fig. S12.

3.7. Microfluidic based ABX-GMFETs

For practical detection of pathogenic bacteria, detection platforms often need to function as dual-channel fluidics with ABX-GMFETs, and the platforms are constructed with a dynamic fluidic system rather than a static system to minimize noise effects from the physical adsorption of bacteria on the transistor and unwanted contaminant interactions. However, most previous studies based on FET geometry have been evaluated under static conditions with no fluid flow interference (Chang et al., 2013; Pourasl et al., 2017; Thakur et al., 2018). Therefore, there are no comparative experimental data, including the actual sensitivity, selectivity, response time and stability, for discriminating bacteria under noisy conditions arising from fluid flow. To evaluate the bacteria-sensing performance of the ABX-GMFETs under a dynamic fluid flow, MEMS processes were redesigned for fluidic modules (Fig. S5). The schematic illustration in Fig. 7A presents the introduction of the mechanisms of GNB and GPB detection. The sensing mechanisms were also explained by electrostatic gating effects: i) at the GNB channel, an interaction between the negative charge of the LPS layer in the outer membrane and the positive charge of the cationic AMPs (right scheme) (Zasloff, 1971) and ii) at the Gram-positive channel, a charge interaction between the D-alanyl-D-alanine moiety at the lipid peptidoglycan terminus and vancomycin (left scheme). In the dynamic fluidic system, the baselines of the ABX-GMFETs were constructed after injection with PBS solution at a constant bias of the source-drain $V_{ds} = -1$ mV and the gate $V_g = -0.1$ V for 200 s (the syringe pump was fixed at a flow rate of 8.3 μL/min). The ABX-GMFET fluidic chip was washed by buffer injection after 350 s to confirm the nonspecific binding effect with current changes. There was no leakage from the flow in the microfluidic channel during the electrical measurement (Kwon et al., 2013). The real-time responses of the ABX-GMFET fluidics are depicted in Fig. 7B–E. The current values depended on the bacteria, and studies were carried out in the presence of various concentrations ranging from 10^1 to 10^3 CFU/mL GNB (*E. coli* and *Salmonella;* Fig. 7B and C) and GPB (*S. aureus* and *E. faecium;* Fig. 7D and E). The intensity values of the ABX-GMFETs were similar to the previous data with a fixed quantity of bacteria: the magainin I-GMFET resulted in higher intensity than that of the vancomycin-GMFET. The baseline was continuously monitored during the liquid flow, and the target bacteria were injected after stabilization with PBS solution. No changes in the signals were observed when using the negative mixture control samples (each gray line in Fig. 7B–E), which indicated the excellent selectivity and sensitivity of the ABX-GMFETs. Although the response intensity increased with increasing target bacteria concentration, the saturation times for the different types of bacteria were dissimilar. To confirm the selectivity of the dual-channel fluidics, the real-time responses in Fig. 7F and G were acquired, showing excellent discrimination between GNB and GPB *via* the dual-channel ABX-GMFETs. The specific responses of the responses was strengthened depending on the additional injection of bacteria. Importantly, the bacteria-discriminating ability of the ABX-GMFETs in dual-channel fluidics was clearly confirmed in Fig. 7H by the sequential injection of four types of bacteria. The real-time responses depicted in the upper part of Fig. 7H show high selectivity for only GNB, while those in the lower part of Fig. 7H exhibit the detection of only GPB. Based on these results, ABX-GMFETs represent, rapid and real-time sensing devices for bacterial discrimination in the context of early pathogen diagnosis.

3.8. Portable ABX-GMFET devices

Various analysis methodologies for bacterial discrimination have been developed; however, there are no customized products because of low sensitivity and selectivity of these methods. To propose the possibility of point-of-care tests, portable ABX-GMFET platforms integrated with fluidics were first demonstrated for healthcare applications (Fig. 8A). The portable ABX-GMFETs incorporate two additional layers: i) a SIM card socket, a microcontroller, power supply, a communication module for outgoing data and an electronic circuit (top layer); and ii) a portable rechargeable battery (bottom layer). In particular, the ABX-GMFET platform integrated with a microfluidic chip was placed in the SIM card socket of the top layer to connect to a syringe pump. The inlet and outlet of the microfluidic chips were connected with a syringe pump *via* a tube for sample injection and flow output, respectively (Fig. 8B). In addition, the microelectrode that physically contacted the microfluidic chip consisted of dual channels for the simultaneous detection of GNB and GPB (Fig. 8C). The optical images of bacteria on the ABX-GMFET dual channel were characterized to observe the presence of the bacteria on the ABX-GMFET platforms after bacterial detection, as shown in the inset of Fig. 8C. Each type of bacteria was injected by the syringe pump at a flow rate of 8.3 μL/min, and the power supplied to the analog-to-digital converter (ADC) was $V_{ds} = -1$ mV (at $V_g = -0.1$ V). As shown in Fig. 8D–G, the real-time responses of the ABX-GMFET fluidic chip to bacteria at concentrations from 10^1 to 10^3 CFU/mL were demonstrated as normalized sensitivities, which were measured based on the current values. Through this approach, the sensing performance of the portable ABX-GMFET system was similar to the results obtained under fluidic conditions, as shown in Fig. 7. In addition, the portable ABX-GMFETs using a microfluidic chip showed excellent reproducibility and repeatability for each bacterium at a concentration of 10^3 CFU/mL (Fig. S13). Therefore, portable ABX-GMFET fluidic chips can be used to discriminate bacteria in real-time monitoring systems.

4. Conclusions

In summary, for the first time, we presented sensitive and selective ABX-GMFET platforms combined with a fluidic chip for the dual detection of coexisting bacteria, namely, GPB and GNB. The ABX-GMFET achieved rapid detection of pathogenic bacteria by conjugation with specific bioprobes, such as vancomycin for GPB species and magainin I for GNB species. Specifically, the ABX-GMFET system was composed of MEMS processes and integrated with novel interfacial chemical compounds and Gram-positive or – negative specific bioreceptors. To investigate the sensing performance of the devices, the ABX-GMFET was incorporated into a liquid-ion-gated system, and its real-time responses to various concentrations of GNB and GPB were monitored. The ABX-GMFETs showed excellent sensitivity and selectivity (LOD: 10^0 CFU/mL) compared to one of previous bacterial biosensors, and their K values were calculated to compare the absorption intensity of the bioprobe-bacterial interactions. Importantly, the ABX-GMFET displayed unprecedented discriminating ability between GNB and GPB. In addition, microfluidics were integrated into the ABX-GMFET system for real-time bacteria detection applications, and the sensing performance of portable system was maintained compared to the bulky-sized ABX-GMFET. Finally, portable devices with a dual-channel ABX-GMFET fluidic chip, which consists of a microchip, an electronic circuit, a communication module and a rechargeable battery, were first demonstrated for point-of-care tests, resulting in a sensing performance similar to that of the liquid-ion-gated ABX-GMFET systems. This technology can potentially be adapted for the on-site monitoring of pathogenic bacteria and for the diagnosis of other types of diseases, such as sepsis, by point-of-care testing.

Author contributions

O.S.K. and S.H.S. initiated the study. K.H.K. and S.J.P. performed the fabrication of sensing platforms, measured the real-time responses, characterizing the sensing electronics and demonstrated sensing mechanism. C.S.P. and J.K. synthesized interfacing chemicals and performed chemical analysis. S.E.S. and J.L. prepared experimental materials and analyzed the experiments. S.H.L. advised MEMS process to design the

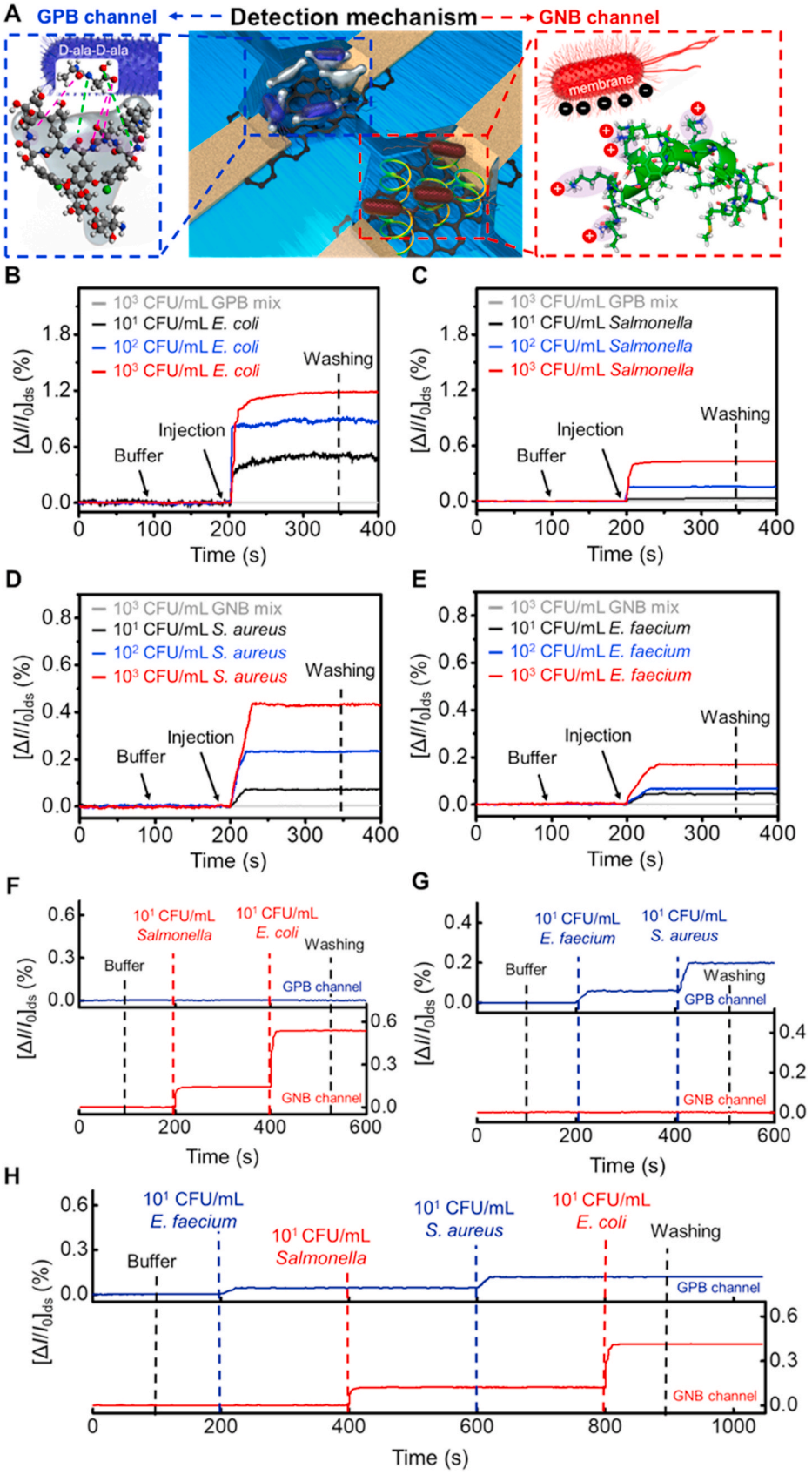

Fig. 7. (A) Schematic diagram of the ABX-GMFET in the dual-channel microfluidics. The extended diagrams indicate each detection mechanism of GPB (left) and GNB (right) in buffer solution. The real-time responses of the ABX-GMFET microfluidics toward various concentrations (10^1–10^3 CFU/mL) of each type of GNB and GPB. The I_{ds} values were measured by the ABX-GMFET toward the following target molecules at V_{ds} = - 1 mV (V_g = - 0.1 V): (B) *E. coli*, (C) *Salmonella*, (D) *S. aureus*, and (E) *E. faecium*. Each GPB mixture and GNB mixture was used as comparison samples. Real-time responses of each ABX-GMFET in dual-channel microfluidics toward (F) GNB, (G) GPB and (H) the mixture with GNB and GPB in buffer solution.

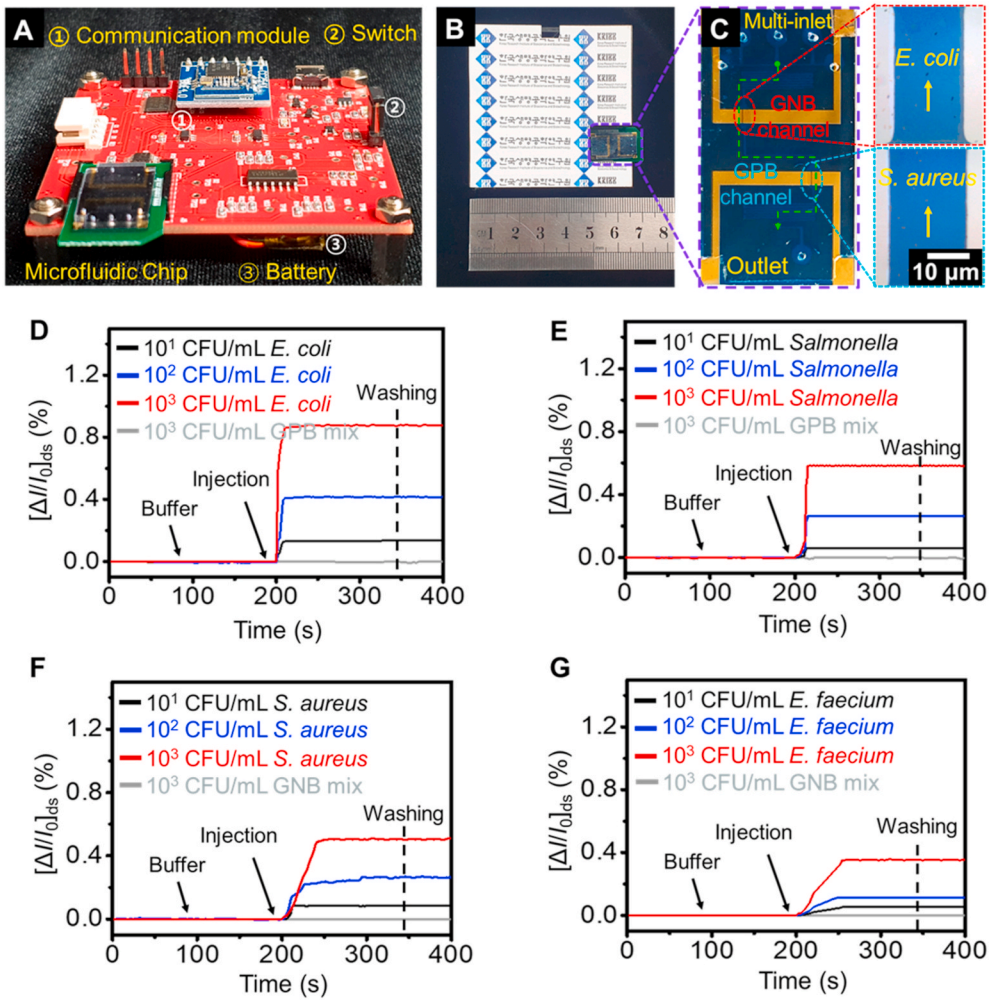

Fig. 8. The point-of-care device with ABX-GMFET microfluidics for detection of bacteria. (A) Front view image of the portable device with 65 mm (width) x 60 mm (depth) x 120 mm (height). (B) Photograph of the packaged portable ABX-GMFET device. (C) Extended photograph of the ABX-GMFET microfluidics on the electrode. Optical images of the bacteria on the ABX-GMFET (inset). The real-time responses of the ABX-GMFET devices to specific target bacteria. The *E. coli*, *Salmonella*, *S. aureus*, and *E. faecium* were used as specific targets for (D) to (G), respectively. Also, the GPB and GNB mixtures at 10^3 CFU/ml as non-target controls were used for (D) and (E), (F) and (G), respectively.

electronics. S.L., J.-S.K. and C.-M. R. incubated the bacteria and prepared target and non-target samples. H.Y. performed DFT calculation. H. S.S provided the information of biomaterials. D.Y. provided cultured bacteria isolated from patients' blood. S.H.L. provided manuscript feedback. O.S.K. conceived and supervised the project and wrote the manuscript.

CRediT authorship contribution statement

Kyung Ho Kim: Methodology, Validation, Writing - review & editing, Data curation. **Seon Joo Park:** Methodology, Validation, Writing - review & editing, Data curation. **Chul Soon Park:** Formal analysis. **Sung Eun Seo:** Formal analysis. **Jiyeon Lee:** Resources, Formal analysis. **Jinyeong Kim:** Resources, Formal analysis. **Seung Hwan Lee:** Methodology. **Soohyun Lee:** Resources. **Jun-Seob Kim:** Resources. **Choong-Min Ryu:** Resources. **Dongeun Yong:** Resources. **Hyeonseok Yoon:** Formal analysis. **Hyun Seok Song:** Conceptualization, Investigation. **Sang Hun Lee:** Writing - review & editing, Data curation, Investigation. **Oh Seok Kwon:** Writing - review & editing, Conceptualization, Supervision, Project administration, Funding acquisition.

Declaration of competing interest

The authors declare that they have no known competing financial interests or personal relationships that could have appeared to influence the work reported in this paper.

Acknowledgments

This work was supported by Korea Institute of Planning and Evaluation for Technology in Food, Agriculture and Forestry (IPET) through Advanced Production Technology Development Program, funded by Ministry of Agriculture, Food and Rural Affairs (MAFRA) (318104-3); The National Research Foundation of Korea (NRF) Grant funded by the Ministry of Science and ICT for First-Mover Program for Accelerating Disruptive Technology Development (NRF-2018M3C1B9069834); The Cooperative Research Program for Agriculture Science and Technology Development, funded by Rural Development Administration (Project No. PJ014790022020); The National Research Council of Science & Technology (NST) grant by the Korea government (MSIP) (No. CPS-19-04-KRIBB) and the KRIBB Initiative Research Program.

Appendix A. Supplementary data

Supplementary data to this article can be found online at https://doi.org/10.1016/j.bios.2020.112514.

References

Allen, M.J., Tung, V.C., Kaner, R.B., 2010. Chem. Rev. 110, 132–145.
An, J.H., Park, S.J., Kwon, O.S., Bae, J., Jang, J., 2013. ACS Nano 7, 10563–10571.
Avouris, P., Dimitrakopoulos, C., 2012. Mater. Today 15, 86–97.
Bolotin, K.I., Sikes, K.J., Jiang, Z., Klima, M., Fudenberg, G., Hone, J., Kim, P., Stormer, H.L., 2008. Solid State Commun. 146, 351–355.
Chang, J., Mao, S., Zhang, Y., Cui, S., Zhou, G., Wu, X., Yang, C.H., Chen, J., 2013. Nanoscale 5, 3620–3626.

Chen, Y., Michael, Z.P., Kotchey, G.P., Zhao, Y., Star, A., 2014. ACS Appl. Mater. Interfaces 6, 3805–3810.
Cuervo, J.H., Rodriguez, B., Houghten, R.A., 1988. Pept. Res. 1, 81–86.
Currie, J., Lin, W., Meng, J., 2014. J. Dev. Econ. 110, 39–51.
Dickson, J.S., Koohmaraie, M., 1989. Appl. Environ. Microbiol. 55, 832–836.
Frank, schwierz, 2010. Nat. Nanotechnol. 5, 487–496.
Fujimoto, T., Awaga, K., 2013. Chem. Chem. Phys. 15, 8983–9006.
García-Aljaro, C., Bangar, M.A., Baldrich, E., Muñoz, F.J., Mulchandani, A., 2010. Biosens. Bioelectron. 25, 2309–2312.
Ghosh, S., Khan, N.I., Tsavalas, J.G., Song, E., 2018. Front. Bioeng. Biotechnol. 6, 1–7.
Gonçalves, F.D.A., de Carvalho, C.C.C.R., 2016. Front. Microbiol. 7, 1–15.
Hu, R., Zhou, F., Zhou, T., Shen, J., Wang, Z., Zhao, Z., Qin, A., Tang, B.Z., 2018. Biomaterials 187, 47–54.
Im, K., Nguyen, D.N., Kim, S., Kong, H.J., Kim, Y., Park, C.S., Kwon, O.S., Yoon, H., 2017. ACS Appl. Mater. Interfaces 9, 10768–10776.
Johnson, J.L.H., Yalkowsky, S.H., 2006. AAPS PharmSciTech 7, E33–E37.
Kennedy, A.D., Otto, M., Braughton, K.R., Whitney, A.R., Chen, L., Mathema, B., Mediavilla, J.R., Byrne, K.A., Parkins, L.D., Tenover, F.C., Kreiswirth, B.N., Musser, J.M., DeLeo, F.R., 2008. Proc. Natl. Acad. Sci. Unit. States Am. 105, 1327–1332.
Kiraly, D.D., Walker, D.M., Calipari, E.S., Labonte, B., Issler, O., Pena, C.J., Ribeiro, E.A., Russo, S.J., Nestler, E.J., 2016. Sci. Rep. 6, 1–12.
Kwon, O.S., Lee, S.H., Park, S.J., An, J.H., Song, H.S., Kim, T., Oh, J.H., Bae, J., Yoon, H., Park, T.H., Jang, J., 2013. Adv. Mater. 25, 4177–4185.
Kwon, O.S., Song, H.S., Park, S.J., Lee, S.H., An, J.H., Park, J.W., Yang, H., Yoon, H., Bae, J., Park, T.H., Jang, J., 2015. Nano Lett. 15, 6559–6567.
Kwon, O.S., Song, H.S., Park, T.H., Jang, J., 2019. Chem. Rev. 1, 36–93.
Lee, B.Y., Sung, M.G., Lee, J., Baik, K.Y., Kwon, Y.K., Lee, M.S., Hong, S., 2011. ACS Nano 5, 4373–4379.
Li, J., McLandsborough, L.A., 1999. Int. J. Food Microbiol. 53, 185–193.
Li, W., Dong, K., Ren, J., Qu, X., 2016. Angew. Chem. Int. Ed. 55, 8049–8053.
Liu, Y., Yuan, L., Yang, M., Zheng, Y., Li, L., Gao, L., Nerngchamnong, N., Nai, C.T., Suchand Sangeeth, C., Feng, Y.P., Nijhuis, C.A., Loh, K.P., 2014. Nat. Commun. 5, 1–8.
Moscicki, B., Shafer, M.A., Millstein, S.G., Irwin, C.E., Schachter, J., 1987. Am. J. Obstet. Gynecol. 157, 65–70.
Moudgil, A., Singh, S., Mishra, N., Mishra, P., Das, S., 2020. Adv. Mater. Technol. 5, 1–11.
Oh, J., Yang, H., Jeong, G.E., Moon, D., Kwon, O.S., Phyo, S., Lee, J., Song, H.S., Park, T. H., Jang, J., 2019. Anal. Chem. 91, 12181–12190.
Ouyang, Z., Zhai, Z., Qin, A., Li, H., Liu, X., Qu, X., Dai, K., 2015. Exp. Ther. Med. 9, 1857–1864.
Pampaloni, N.P., Lottner, M., Giugliano, M., Matruglio, A., D'Amico, F., Prato, M., Garrido, J.A., Ballerini, L., Scaini, D., 2018. Nat. Nanotechnol. 13, 755–764.
Park, S.J., Kwon, O.S., Lee, S.H., Song, H.S., Park, T.H., Jang, J., 2012. Nano Lett. 12, 5082–5090.
Park, S.J., Yang, H., Lee, S.H., Song, H.S., Park, C.S., Bae, J., Kwon, O.S., Park, T.H., Jang, J., 2017. ACS Nano 11, 5950–5959.
Ping, J., Vishnubhotla, R., Vrudhula, A., Johnson, A.T.C., 2016. ACS Nano 10, 8700–8704.
Pourasl, A.H., Ahmadi, M.T., Rahmani, M., Ismail, R., 2017. J. Nanosci. Nanotechnol. 17, 601–605.
Romero, R., Emamian, M., Quintero, R., Wan, M., Hobbins, J.C., Mazor, M., Edberg, S., 1988. Am. J. Obstet. Gynecol. 159, 114–119.
Rybak, M.J., Cappelletty, D.M., Moldovan, T., Aeschlimann, J.R., Kaatz, G.W., 1998. Antimicrob. Agents Chemother. 42, 721–724.
Seo, D.H., Pineda, S., Fang, J., Gozukara, Y., Yick, S., Bendavid, A., Lam, S.K.H., Murdock, A.T., Murphy, A.B., Han, Z.J., Ostrikov, K., 2017. Nat. Commun. 8, 14217.
Shai, Y., 1999. Biochim. Biophys. Acta Biomembr. 142, 55–70.
Singh, S., Moudgil, A., Mishra, N., Das, S., Mishra, P., 2019. Biosens. Bioelectron. 136, 23–30.
Smith, P.A., Koehler, M.F.T., Girgis, H.S., Yan, D., Chen, Yongsheng, Chen, Yuan, Crawford, J.J., Durk, M.R., Higuchi, R.I., Kang, J., Murray, J., Paraselli, P., Park, S., Phung, W., Quinn, J.G., Roberts, T.C., Rougé, L., Schwarz, J.B., Skippington, E., Wai, J., Xu, M., Yu, Z., Zhang, H., Tan, M.W., Heise, C.E., 2018. Nature 561, 189–194.
Song, H.S., Kwon, O.S., Lee, S.H., Park, S.J., Kim, U.K., Jang, J., Park, T.H., 2013. Nano Lett. 13, 172–178.
Soni, K.A., Balasubramanian, A.K., Beskok, A., Pillai, S.D., 2008. Curr. Microbiol. 56, 93–97.
Takacsnovak, K., Noszal, B., Tokeskovesdi, M., Szasz, G., 1993. Int. J. Pharm. 89, 261–263.
Thakur, B., Zhou, G., Cdddhang, J., Pu, H., Jin, B., Sui, X., Yuan, X., Yang, C.-H., Magruder, M., Chen, J., 2018. Biosens. Bioelectron. 110, 16–22.
Ugolini, M., Gerhard, J., Burkert, S., Jensen, K.J., Georg, P., Ebner, F., Volkers, S.M., Thada, S., Dietert, K., Bauer, L., Schäfer, A., Helbig, E.T., Opitz, B., Kurth, F., Sur, S., Dittrich, N., Gaddam, S., Conrad, M.L., Benn, C.S., Blohm, U., Gruber, A.D., Hutloff, A., Hartmann, S., Boekschoten, M.V., Müller, M., Jungersen, G., Schumann, R.R., Suttorp, N., Sander, L.E., 2018. Nat. Immunol. 19, 386–396.
Vaisocherová-Lísalová, H., Víšová, I., Ermini, M.L., Špringer, T., Song, X.C., Mrázek, J., Lamačová, J., Scott Lynn, N., Šedivák, P., Homola, J., 2016. Biosens. Bioelectron. 80, 84–90.
Wakshlak, R.B.K., Pedahzur, R., Avnir, D., 2015. Sci. Rep. 5, 1–5.
Walsh, C.T., 1993. Science 261, 308–309.
Wang, R., Kim, K., Choi, N., Wang, X., Lee, J., Jeon, J.H., Rhie, G. eun, Choo, J., 2018. Sensor. Actuator. B Chem. 270, 72–79.
Wu, G., Dai, Z., Tang, X., Lin, Z., Lo, P.K., Meyyappan, M., Lai, K.W.C., 2017. Adv. Healthc. Mater. 6, 1–9.
Zasloff, Michael, 1971. University of Toronto Press, Toronto, pp. 389–395.